ACES Asian Chemical Editorial Society

doi.org/10.1002/asia.202401798

CHEMISTRY AN ASIAN JOURNAL Research Article

www.chemasianj.org

Probing the Slow Relaxation of Magnetization of a Square Planar Cobalt Complex with Doublet Ground State

Kamal Uddin Ansari[+],[a] Dipanti Borah[+],[a] Amaleswari Rasamsetty,[a] Pardeep Kumar,[a] Muralidharan Shanmugam,[b] Gopalan Rajaraman,*[a] and Maheswaran Shanmugam*[a]

The observation of slow relaxation of magnetization in low-spin square planar cobalt complexes is exceedingly rare, likely due to the synthetic challenges of stabilizing such geometries, along with the complexities introduced by hyperfine interactions and spin-orbit coupling. Additionally, accurately characterizing the ground-state electronic configuration of these complexes remains a significant challenge. In this article, we report a unique and rare square planar cobalt complex, $[Co(L1^{\bullet-})_2]$ (**1**), where the coordination sites are occupied by the phenanthroiminoquinone (L1). The molecular structure of complex **1** was determined using single-crystal X-ray diffraction studies. A structurally analogous nickel complex, $[Ni^{II}(L1^{\bullet-})_2]$ (**2**), was also synthesized and characterized. Detailed DC magnetic susceptibility measurements of **2** reveal strong antiferromagnetic exchange interactions between the radical centers, rendering it diamagnetic. For cobalt complex **1**, this strong antiferromagnetic coupling results in a doublet ground state, as corroborated by X-band EPR measurements (at 5 K) conducted on both polycrystalline and frozen solution samples. To gain deeper insights into the electronic structure of the cobalt ion in **1**, a comprehensive suite of experimental and theoretical investigations was conducted, including X-ray diffraction, DC magnetic studies, X-band EPR, UV-Vis-NIR spectroscopy, and ab initio calculations. These studies collectively indicate that the cobalt ion in **1** exists in a divalent low-spin state. Furthermore, the observed slow relaxation of magnetization for the doublet state of **1** highlights its potential as an ideal candidate for designing spin-based molecular qubits.

Introduction

The two prominent properties of the pincer-based ligand, namely deprotonation and redox non-innocence, are dominantly exploited to isolate 3d- transition metal complexes with various coordination geometries. This approach led to the isolation of metal complexes with distinct electronic and magnetic properties, which are mainly targeted for a variety of catalytic reactions such as small molecule activation, solar fuel, catalyst, artificial photosystems,[1] epoxidation of alkenes, co-polymerisation of CO_2, asymmetric synthesis,[2] olefin polymerisation, hydrogenation, hydroboration,[3] and hydroamination reaction, etc.[4] The change in electronic structure (e.g., the spin state of the metal ion) appears to be the key to the observed catalytic activity in these complexes, where a change in spin state is easily accommodated by the redox non-innocent ligand, i.e., the integral cooperative effect between the metal and the coordinated ligand.[4b,5]

Metal complexes featuring pincer backbones or other redox non-innocent ligands are of interest not only for catalysis but also for their intriguing magnetic properties. For instance, studies have highlighted the complexities in accurately determining the electronic structures of such systems.[3d,6] A notable example is an octahedral Co(II) complex with redox-active bis(iminopyridyl) radical chelate ligands, where the exchange coupling between the radicals on the two ligands dominates, yielding a quartet ground state. In contrast, the Fe(II) analogue of this Co(II) complex exhibits a triplet ground state, driven by stronger Fe(II)-radical exchange compared to radical-radical coupling.[7] Interestingly, a square planar Co(II) complex with bis(iminopyridyl) radical chelate ligands presents a singlet ground state. This arises from antiferromagnetic coupling between the low-spin Co(II) center and the radical chelate, as reported in an unrelated study.[8] These findings underline the diverse magnetic behaviors achievable with such ligand systems and the nuanced interplay of electronic interactions that govern them.

Among the various transition metal-based Single-ion magnets (SIM), Co(II) complexes (with various ligands including redox-active ligands) possess an edge over the other complexes due to i) the large orbital angular momentum, ii) spin-orbit coupling, and iii) Kramers' ion.[9] These factors constitute a large magnetic anisotropy that has a non-zero influence on the magnitude of the effective energy barrier, which in turn correlates to the blocking temperature. Besides the classical signature of a magnet, Single-molecule magnets (SMM) or SIM show quantum mechanical phenomenon and are therefore

[a] *Dr. K. U. Ansari,[+] D. Borah,[+] Dr. A. Rasamsetty, Dr. P. Kumar, Prof. Dr. G. Rajaraman, Prof. Dr. M. Shanmugam*
Department of Chemistry
Indian Institute of Technology Bombay
Powai, Mumbai, Maharashtra 400076, India
E-mail: eswar@chem.iitb.ac.in
rajaraman@chem.iitb.ac.in

[b] *Dr. M. Shanmugam*
EPSRC National Research Facility (NRF)
Department of Chemistry and Photon Science Institute
The University of Manchester
Manchester M13 9PL, U.K.

[+] *These authors contributed equally.*

Supporting information for this article is available on the WWW under https://doi.org/10.1002/asia.202401798

envisaged as a potential system to build efficient Spin Qubit.[10] However, to realise the entangled state, the phase memory time (T_2) should be large, which is often a challenge to control and/or manipulate.[11]

Researchers have focused on molecular complexes with well-isolated doublet ground states, where the first excited state is separated by several hundred or thousand cm^{-1}. Such isolation is expected to result in a significantly long T_2. For instance, certain vanadyl ion-based molecular qubits have demonstrated impressive T_2 values, reaching up to 1 μs even at room temperature.[11b–f,12]

Only a handful of metal complexes (such as Cu(II), Mn(V), V(IV), etc.) with the doublet ground state exhibit slow relaxation of magnetisation.[11–13] However, Co(II) complexes with doublet ground state exhibiting slow relaxation of magnetisation are extremely scarce in the literature compared to their high-spin congener.[14] In this report, we show a synthetic strategy to stabilise cobalt ion in its square planar geometry using exclusively a bidentate redox non-innocent ligand, namely, phenanthroiminoquinone (L1). The single crystal x-ray structure determination reveals that the coordination sites of the cobalt ion were completed by two bidentate L1 ligands (**1**, Scheme 1). To elucidate the electronic structure of **1**, we performed DC magnetic susceptibility and X-band EPR studies. The magnetization relaxation dynamics were investigated through AC susceptibility measurements. Furthermore, theoretical calculations were carried out not only to gain deeper insight into the electronic structure of **1** but also to validate and support the experimental findings.

Results and Discussion

Structural Description of 1

The reaction of two equivalents of L1 with one equivalent of $[Co(PMe_3)_4]$ in dry THF led us to isolate violet colour block-shaped single crystals of **1** (see scheme 1).

Complex **1** crystallises in the orthorhombic, *Pccn* space group (Figure 1, see Table S1 of ESI). The asymmetric unit of **1** consists of half of the molecule and the remaining fragment was generated by inversion symmetry. In **1**, the cobalt ion coordination sites were completed by two bidentate L1 (N_2O_2),

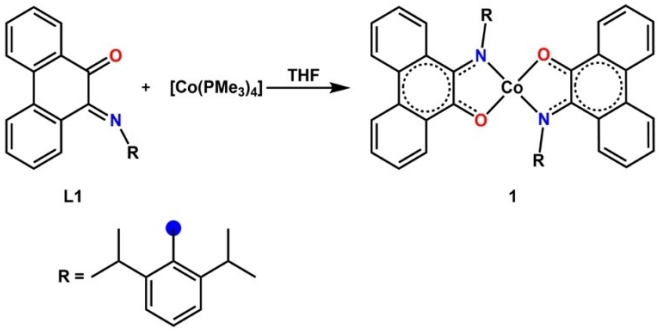

Scheme 1. The synthetic procedure followed to isolate **1**.

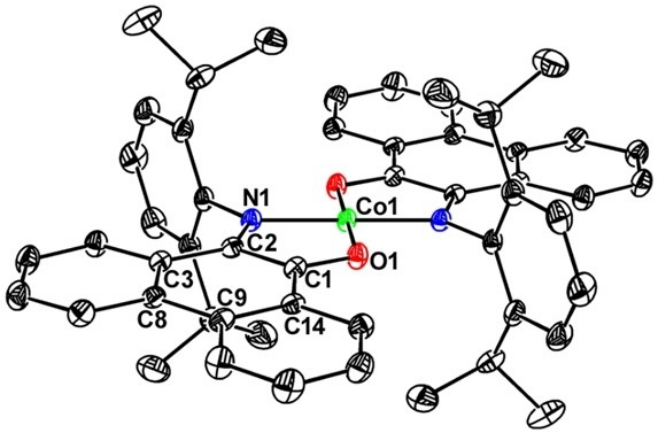

Figure 1. Molecular structure of **1**. Colour code: Co = Green, O = red, N = blue, C = black. All the hydrogens have been removed for clarity. Selected bond lengths: Co1-O1 = 1.8226(15) Å, Co1-N1 = 1.8475(19) Å, C1-O1 = 1.309(3) Å, C1-C2 = 1.410(3) Å, C2-N1 = 1.371(6) Å and bond angles: O1-Co1-O1# = 180°, N1-Co1-N1# = 180°, O(1)-Co(1)-N(1)#1 = 94.91(8)°, O(1)-Co-(1)-N(1) = 85.09(8)°.

and it exists in distorted square planar geometry which is evidently reflected from the bite angle N1-Co1-O1 of 85.1(2)° in **1**. However, no distortion is observed in the *trans*-bond angle O1-Co1-O1#, and the N1-Co1-N1# is equal to 180°. The Co1-O1 and Co1-N1 bond lengths were observed to be 1.8226(5) Å and 1.8475(5) Å, respectively.[15] The 2,6-diisopropyl phenyl substituent on the N-atom of L1 lies orthogonal to the N_2O_2 plane, thus preventing any other ligand from approaching from the axial direction; hence a square planar geometry around the cobalt centre is easily accomplished (see Table S2 of ESI).

To gain a deeper understanding of the electronic structure of complex **1**, we analyzed the bond lengths of the redox-active ligand L1 coordinated to the cobalt ion.Notably, the bond length of C1–O1 (1.309(4) Å) and C2–N1 (1.371(6) Å) are elongated, while the C1–C2 bond (1.410(3) Å) is slightly shortened compared to its neutral counterpart. These changes align with the expected structural modifications upon one-electron reduction of L1. The complete bond lengths and bond angles for complex **1** are detailed in Tables S3 and S4 of ESI. The observed C1–O1 and C2–N1 bond lengths closely match those reported for the one-electron-reduced form of L1 (refer to Scheme 2). Furthermore, the absence of counterions or solvate molecules, in the crystal lattice, combined with bond valence sum (BVS) calculations (see Table S5 of ESI and related text), confirms that the cobalt ion in **1** exists in a divalent oxidation state.

Electron Paramagnetic Resonance Studies of 1

To further shed light on the electronic structure of **1**, variable temperature, CW X-band EPR measurements (5–50 K) was performed on both the frozen solution (in toluene) and the polycrystalline powder of **1** (see Figure S1 of ESI). In both the cases, well-resolved, axial-like EPR signals are observed. The toluene frozen solution of **1** shown in Figure 2 shows a nicely

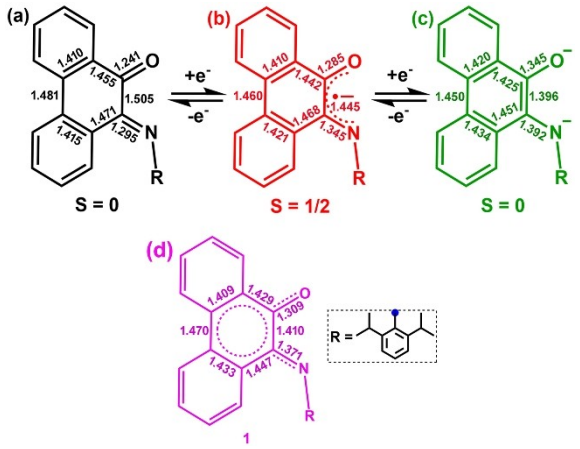

Scheme 2. The bond lengths of (a) neutral, (b) 1 e^- and (c) 2 e^- reduced L1 ligands of the reported metal complexes. d) The bond lengths observed in **1**.

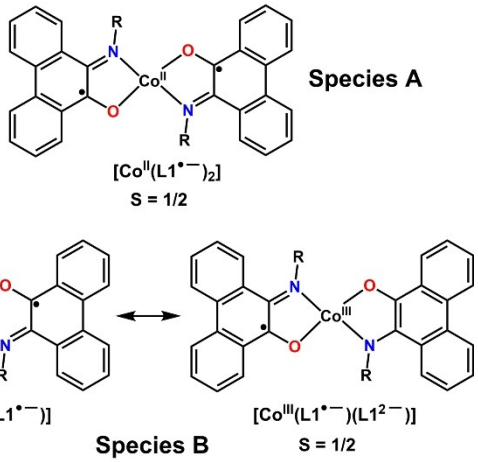

Scheme 3. Possible resonance states of Complex **1**.

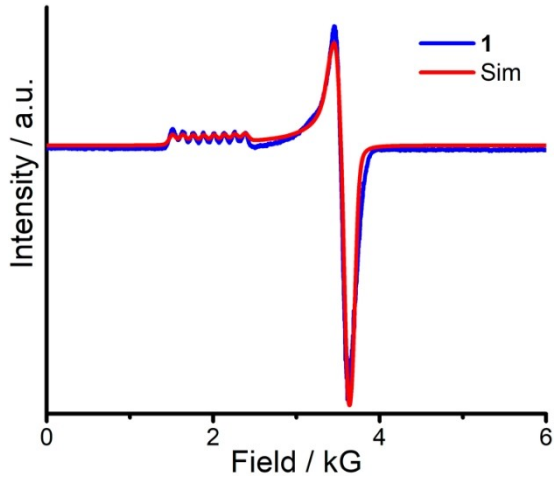

Figure 2. The X-band EPR spectrum of a frozen toluene solution of **1** measured at 5 K (blue trace). The solid red line represents the simulation of the experimental data using the parameters described in the main text. Experimental conditions: frequency = 9.3846 GHz, modulation amplitude = 0.4 mT; microwave power = 0.6325 mW, (attenuation = 25 dB), lw = [8, 3.3] mT.

resolved eight-line hyperfine pattern along the $g_{||}$ region due to the interaction of the unpaired electron spin ($S = 1/2$) of the Co(II) ion with the nuclear spin ($I = 7/2$) of the ^{59}Co nucleus while relatively sharp $g_{\perp}$ signals are observed in the $g = 2$ regions.

The EPR spectral feature obtained for both polycrystalline and frozen solution of **1** resembles that of several low-spin Co(II) complexes reported in the literature. Alternatively, a spin doublet state may arise due to a strong antiferromagnetic coupling between a Co(III) ion ($S = 1$) and the paramagnetic L1 ($S = 1/2$; see Scheme 3). However, single crystal X-ray diffraction, the DC magnetic data and computational calculations reveal (*vide infra*) that **1** predominantly exists in the Species A form given in Scheme 3.

The experimental EPR spectrum (blue trace) was simulated (red trace) by considering the following spin-Hamiltonian parameters; $S = 1/2$, $g = [1.86, 1.9, 3.44]$, $\mathbf{A}(^{59}Co) = [50, 50, 600]$ MHz, linewidths = [8, 3.3] mT using easy-spin software.[16] The strong ^{59}Co hyperfine coupling (600 MHz) observed at $g = 3.44$ implies that the unpaired electron density is predominantly localised on the cobalt ion of **1**. Further, the large **"g"** anisotropy observed for **1** is likely associated with the significant spin-orbit coupling contribution to the ground state of **1**. A similar scenario has been reported previously for other Co(II) low-spin square planar complexes.[3j,17]

Direct Current Magnetic Susceptibility Studies of 1

Further to understand the electronic structure of **1**, dc magnetic susceptibility measurements were performed on the polycrystalline sample of **1**, in the temperature range of 2–300 K in the presence of 1 kOe magnetic field (see Figure 3). The observed room temperature $\chi_M T$ value of 0.75 $cm^3 mol^{-1}$ K which is significantly smaller than the expected $\chi_M T$ value for a high-spin Co(II) ($g = 2$; $\chi_M T = 1.875$ $cm^3 mol^{-1}K$) or a low-spin Co(II) and two uncoupled radical ligands ($g = 2$; $\chi_M T = 0.375$ $cm^3 mol^{-1}K$ for each radical) or Co(III) ($S = 1$) and an uncoupled radical ligand ($g = 2$; $\chi_M T = 0.375$ $cm^3 mol^{-1}K$). This implies a strong intramolecular antiferromagnetic coupling between the paramagnetic centres in **1**. Upon lowering the temperature, the $\chi_M T$ value decreases gradually up to 25 K. Below this temperature, the $\chi_M T$ value drops suddenly to reach a final value of 0.48 $cm^3 K mol^{-1}$.

To better understand the nature of the electronic structure of **1**, we have attempted to synthesise the Ni(II) analogue of complex **1** (complex **2**) for the following reasons i) to understand the nature and strength of the exchange coupling between the radical ligands, ii) to infer the nature of exchange coupling between the radical and cobalt ion iii) to disclose the spin state of cobalt ion, i.e., high-spin or low-spin.

An attempt to isolate the single crystals of nickel analogue of **1** failed, but always a polycrystalline material was obtained despite trying various crystallisation techniques with the

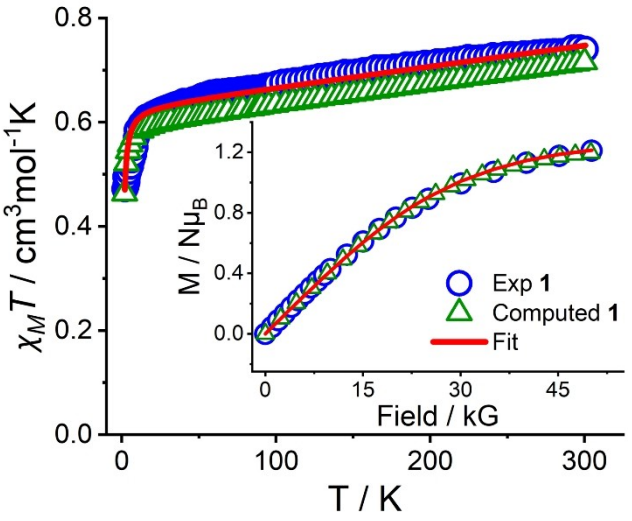

Figure 3. Temperature-dependent magnetic susceptibility measurement of **1** in the presence of 1 kOe external magnetic field. Inset: Field dependent-magnetization measurement of **1** performed at 2 K in the field range of 0–50 kOe. Solid red lines represent simulation using the parameter described in the text.

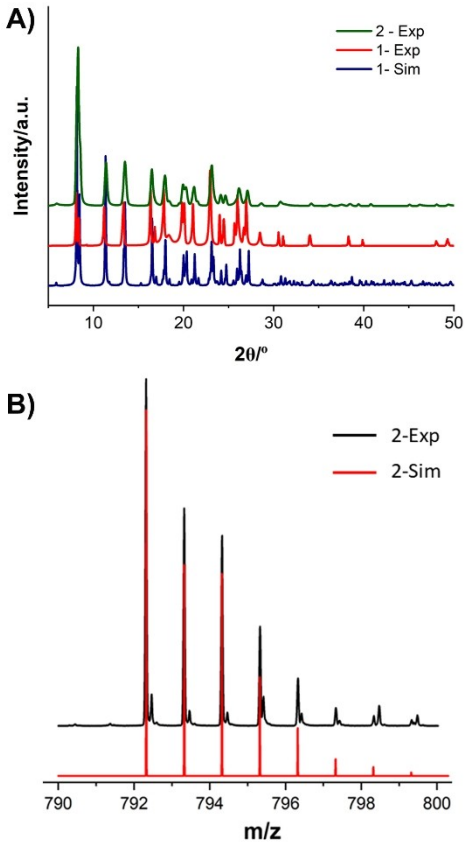

Figure 4. A) Powder X-ray diffraction pattern of **1** and **2**, B) ESI-Mass spectrum of **2**.

innumerable solvent combination (see the experimental section for details).

However, to our pleasant surprise, the powder X-ray diffraction pattern of the polycrystalline material of **2** obtained (green trace in Figure 4A) is in excellent agreement with the PXRD profile of **1**, which was generated from its single-crystal X-ray data (blue trace Figure 4A). Further, the ESI-MS data of this nickel complex shows an m/z value of 792.315 g/mol (see Figure 4B). To determine further the oxidation state of the nickel ion in **2** unambiguously, we have performed x-ray photoelectron spectroscopy (XPS) measurements. We observed the x-ray photoelectron lines of Ni $2P_{3/2}$ and $2P_{1/2}$ at 854.1 eV and 871.4 eV respectively (see Figure S2 of ESI). The observed peak positions evidently imply that the oxidation state of nickel ion is in +2, which is in excellent agreement with the literature report.[18] Based on the XPS, ESI-MS and PXRD data one can safely represent the molecular formula and the electronic structure of the nickel complex as [Ni(L1$^{\bullet-}$)$_2$] (**2**). In such a nickel complex, due to its inherent electronic structure, the two redox non-innocent ligands are valence localised. This has been elegantly established in an unrelated literature report earlier.[15a] To confirm the thermal stability of **1** and **2**, we have performed thermogravimetric analysis up to 873 K. This measurement reveals that **1** and **2** are stable up to 550 K and 470 K, respectively (see Figure S3 of ESI).

Variable temperature magnetic susceptibility measurements were performed on a polycrystalline sample of **2** in the presence of 1 kOe external magnetic field. The $\chi_M T$ value of **2** was observed to be zero in the entire temperature range measured 2–300 K (see Figure S4 of ESI). This firmly indicates that the two radicals in **2** coupled antiferromagnetically, and their exchange strength is comparable to that of the thermal energy at room temperature. Extending this finding to the magnetic data measured for **1** discloses the following i) the magnetic moment contribution of the two radicals in **1** to the overall magnetic moment is zero (assuming the electronic structure of A in Scheme 3) ii) the Co(II) ion in **1** exists as a low-spin with the significantly large g-anisotropy, which presumably arises from the spin-orbit coupling. This is well corroborated with the EPR spin Hamiltonian parameters extracted.

In an unrelated report, it's been shown that the radical-radical exchange coupling dominates over Co(II)-radical exchange coupling in an octahedral Co(II) complex of bis(iminopyridyl)chelate radical ligands.[7a] While the scenario drastically changes when replacing the octahedral Co(II) ion with Fe(II) ion, *i.e.*, Fe(II)-radical coupling strength is stronger than the radical-radical coupling in this case.[7b] On the other hand, square planar complexes of the general formula of [(BIP)CoX] (where X=H or Cl or Me; BIP: bis(iminopyridine) chelate radical) exhibit an overall singlet ground state due to the antiferromagnetic coupling between the low-spin Co(II) and the BIP radical ligand.[7a,19] A large magnetic moment is always witnessed for other low-spin Co(II) square planar complexes which are consistent with our observation.[20]

Further, we have performed an isothermal magnetisation measurement upon sweeping the external magnetic field up to 50 kOe. The magnetic moment of complex **1** reaches approximately 1.2 Nμ$_B$ at 50 kOe (2.0 K). This slightly elevated magnetic moment can be attributed to the significant g-anisotropy

observed, consistent with the EPR data. These findings confirm that **1** possesses a doublet ground state.

Considering the complex electronic structure possessed by **1**, an antiferromagnetic coupling between a triplet Co(III) ion and a radical ligand in a square planar complex cannot be neglected (assuming the electronic structure of B in Scheme 3). Based on this information, we have attempted to model the magnetic data of **1** in two ways i) considering only the spin state of the Co(II) ion (assuming the electronic structure of A given in Scheme 3, where the two radicals contribute to the total magnetic moment is zero due to the strong antiferromagnetic coupling as observed in **2**); ii) an antiferromagnetic coupling between a triplet Co(III) and a radical ligand. Compared to the latter model, the former model gives an excellent fit (simultaneous fit of both $\chi_M T(T)$ and $M(H)$) to the experimental data ($H = g\mu_B S.H + zJ\langle S_z\rangle S_z$)[21] using $S = 1/2$, g_x, $g_y = 1.98$, $g_z = 3.50$ and $zJ = -0.59\ cm^{-1}$ where zJ = intermolecular exchange interactions. The extracted spin-Hamiltonian (SH) parameters closely align with those obtained from EPR measurements (*vide supra*). Furthermore, SH parameters computed for $[Co^{II}(L1^{\bullet-})_2]$ (*vide infra*) using DFT/ab initio methods also reproduce the experimental magnetic data (Table 1). These results confirm that the low-spin divalent cobalt ion is coordinated with the singly reduced radical anion of L1.

Next, we investigated the absorption profiles of both **1** and **2** and the UV-Vis-NIR profile was recorded in dry THF solvent at room temperature. Both complexes show a similar absorption profile indicative that both complexes are likely to be structurally analogue to each other, which is consistent with the finding from PXRD measurements. Complex **1** (**2**) shows bands at 967 (955) nm, 587 (615) nm, and a couple more peaks in the UV region. The presence of a NIR band around 1000 nm for both **1** and **2** (red and blue trace in Figure 5),[15b,c] which is evidently absent in the metal-free neutral L1 ligand (green trace in Figure 5), indicative of the paramagnetic signature associated with L1. The TD-DFT calculations (employing B3LYP functional, see computational details for more information) were performed to understand the nature of the transition involved in these complexes. The computed UV-Vis-NIR spectra are in reasonable agreement with the experimental data. Also, the calculations unveil that all the transitions observed in the spectra correspond to predominantly ligand-to-ligand charges (LLCT) and ligand-to-metal charge transfer (LMCT) transitions (see Figure 5 for details). The absorption profile of both **1** and **2** resembles that of certain square planar complexes reported in the literature.[15a,b]

Table 1. Comparison of SH parameters obtained for **1**.

SH parameters	Experimental		Computed
	EPR	DC data	
S	1/2	1/2	1/2
g_x	1.86	1.98	1.96
g_y	1.90	1.98	2.29
g_z	3.44	3.50	3.16

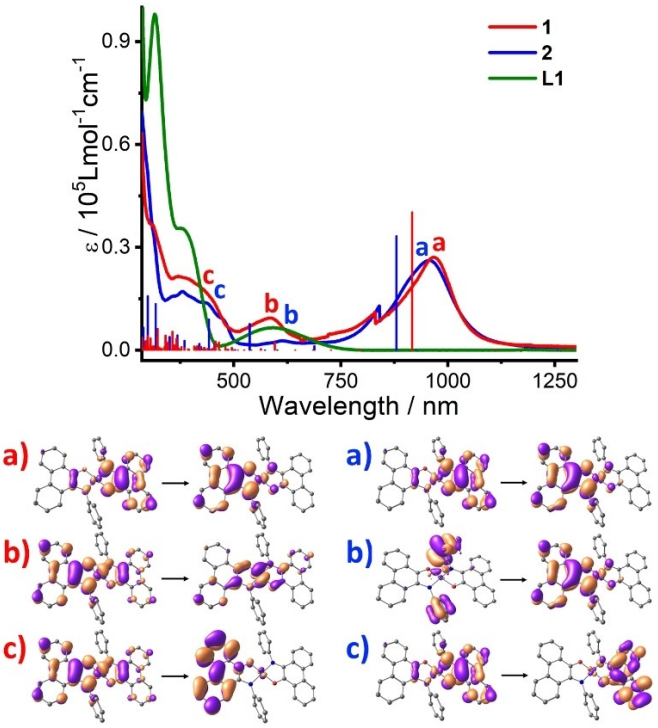

Figure 5. The UV-Vis spectra of complexes **1** and **2** (1.5×10^{-5} M) and L1 (1.2×10^{-5} M) recorded in THF solvent at room temperature (top panel) and HOMO-LUMO transition of **1** (bottom left panel) and **2** (bottom right panel). The MOs were plotted using an iso-surface value of 0.03.

The experimental absorption features seen in ~967 and 955 nm for **1** and **2** were reproduced in the TD-DFT calculations (915 nm and 881 nm, respectively) and were assigned as intra-ligand charge transfer transitions mediated via d_{xz}/d_{yz} orbital of the metal, as described earlier.[15a,b,22] The metal MO contributions for the Cobalt are found to be larger compared to the Nickel (24% vis-à-vis 9%). This suggests that the transition observed in Co complexes are metal centric, while for the Ni complexes, ligands play a critical role in the absorption features observed.

Theoretical Calculations on 1

To understand in detail the electronic structure of the complex, we first performed DFT calculations using B3LYP/TZVP setup (see the Computational details section). Since there are two possible electronic structures for **1** as shown in scheme 3, we have decided to perform single-point calculations on the X-ray geometry to obtain the correct electronic structure. Otherwise, the gas phase geometry optimisation can lead to other isomers which usually ignore the solid-state effects. Calculations yield $S = 1/2$ as the ground state with the $S = 3/2$ state found to be only 15.8 kJ/mol, affirming the experimental observations that the ground is doublet arising from strong radical-radical antiferromagnetic interaction.[23]

The DFT computed spin density on the $S = 1/2$ state reveals a net spin density of ~1.1, ~-0.99 and ~+0.99 on two radical

centres suggesting a dominant Co(II) character (see Figure 6A). Therefore, to understand in detail the oxidation state of the cobalt ion, we have analysed the spin density of the S = 3/2 state. As spin density at the cobalt centre is strongly influenced by the delocalisation of spin density from the ligands, the S = 1/2 state having $\mathbf{L^{\bullet\downarrow}}$–$\mathbf{Co^{II\uparrow}}$–$\mathbf{L^{\bullet\uparrow}}$ does not yield a complete picture of the total spin density at the cobalt centre. On the other hand, for the S = 3/2 state, the spin density on the cobalt centre was found to be ~1.3 (see Figure S5 of ESI), suggesting that the oxidation state of Co is +2 in the low-spin state. Further, we have plotted the frontier molecular orbitals (MOs) of the S = 1/2 state, which also implies a similar electronic structure (see Figure 7).

As Co(II) is the dominant factor that contributes to the ground state electronic structure, also affirmed from magnetic data and the single crystal x-ray data, we have performed limited reference space CASSCF/NEVPT2 calculations CAS(7,5) (see Computational details section) to understand the ligand field splitting at the Co(II) centre. The AILFT computed orbital is shown in Figure S6 of ESI. As expected, the d_{z^2} orbital is found to be the lowest lying with the unpaired electron found to be localised on the d_{yz} orbital.[24] The CASSCF/NEVPT2 computed g-tensors are [1.96, 2.29, 3.16] in good agreement with the parameters extracted from EPR data [1.86, 1.9, 3.44] and magnetic data fit [1.96, 1.96, 3.50], offering confidence in the computed parameters (Table 1).

On the other hand, for the model Ni complex, the spin density observed at the nickel center is 0.00 implying that the metal ion is in a low-spin divalent oxidation state and the radicals on ligands are coupled antiferromagnetically (see Figure 6B). This is consistent with the variable temperature magnetic studies performed on **2**. The detailed investigation of the Eigen-value plot suggests that there is no metallic character near the frontier molecular orbitals (see Figure S7 of ESI).[25]

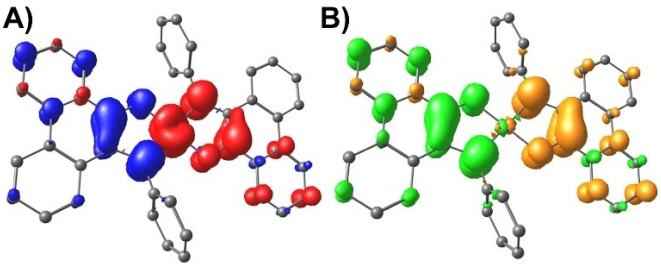

Figure 6. DFT computed spin density plot of A) **1** (S = 1/2) and B) **2** (S = 0) states with an iso-surface value of 0.0026. Here blue and green represent negative spin density, while red and orange represent positive spin density.

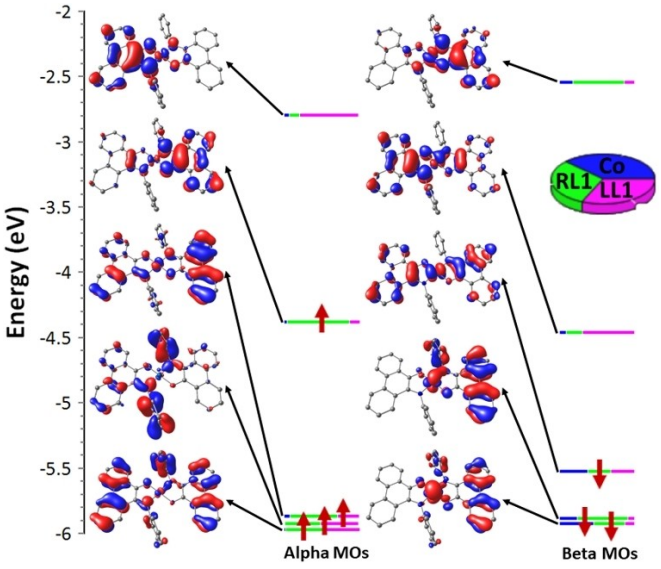

Figure 7. DFT computed frontier molecular orbitals of **1** (S = 1/2) along with the percent decomposition for metal and radical ligands (RL1 (right L1) and LL1 (left L1)). The MOs were plotted using an iso-surface value of 0.03.

Magnetisation Relaxation Dynamics of 1

To gain more insight into the magnetic relaxation process, we performed the ac magnetic susceptibility measurement for **1** in the temperature range of 1.9–3.2 K in the presence of 3.5 Oe oscillating magnetic field. No out-of-phase signal has been observed in the absence of an external magnetic field, which is not surprising for a system with a doublet ground state.[14a,b,26] From the field sweep measurements (see Figure S8 of ESI), we noticed the relaxation is slower at 1 kOe external magnetic field. At this optimum field, ac susceptibility measurements were performed on the polycrystalline samples of **1**, which shows out-of-phase susceptibility signals (see Figure S9 of ESI). The Cole-Cole plot has been fitted by employing the generalised Debye model (Equation 1; see Figure 8A), considering a single relaxation process.[27]

$$\chi(\omega) = \chi_s + \frac{\chi_T - \chi_s}{1 + (i\omega\tau)^{1-\alpha}} \quad (1)$$

In the above equation, χ_s, χ_T, ω, and τ are adiabatic susceptibility, isothermal susceptibility, angular frequency, and relaxation time, respectively. The extracted α values are in the range of 0.31-0.14, indicative of the narrow distribution of relaxation time.[28] The parameters employed to fit the Cole-Cole plots of **1** are listed in Table S6 of ESI.

The relaxation time derived from the Cole-Cole fit of **1** was used to construct the Arrhenius plot (see Figure 8B). Figure 8B discloses that the Arrhenius curve deviates from the linearity in the entire temperature range measured. The data were fitted by considering only the Direct and Raman processes (Equation 2). A good agreement between the fit and the experimental data was obtained using the A = 33.36 $kOe^{-2}K^{-1}s^{-1}$, C = 0.28 $s^{-1}K^{-n}$ and n = 5.90, and the extracted parameters are consistent with the literature reports.[11e,14,26,29] For Kramers' doublet, the expected exponent for the Raman process is n = 9; a significant deviation that is indicative of the involvement of both optical and acoustic phonon processes.

$$\frac{1}{\tau} = AH^2T + CT^n \quad (2)$$

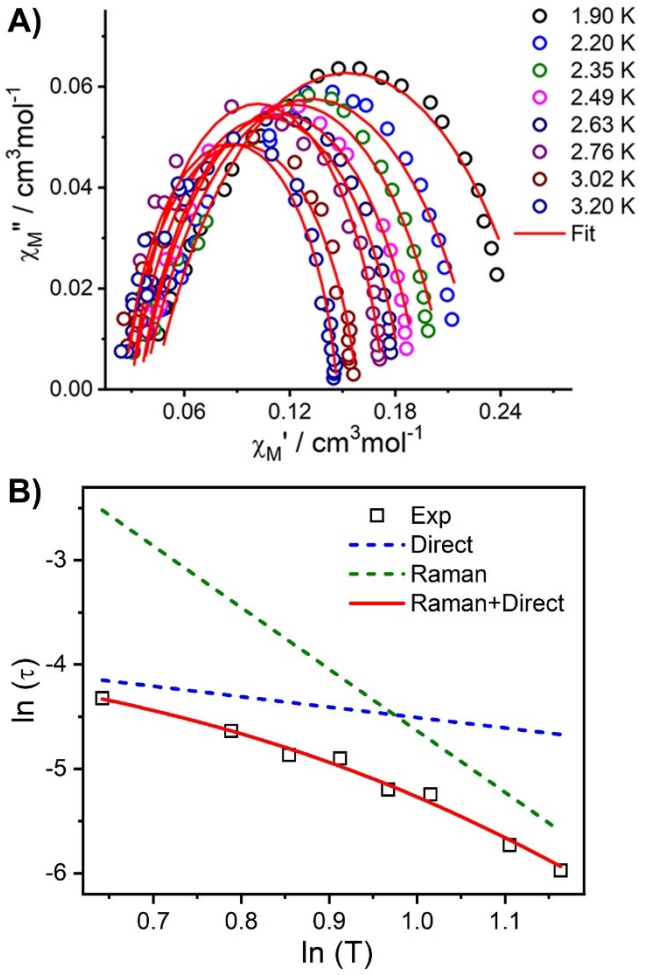

Figure 8. A) Cole-Cole plot of **1** measured in the presence of 1 kOe of the external magnetic field at the indicated temperature. The solid line represents the best fit with the parameter described in the text. B) Arrhenius plot of the natural log of the relaxation time, τ, versus the natural log of temperature. The red line represents the best fit with the parameter described in the text.

Slow relaxation of magnetisation is often observed for the system with strong magnetic anisotropy with a ground state $S > 1/2$. However, observation of slow relaxation of magnetisation with an $S = 1/2$ ground state is relatively scarce compared to the systems with $S > 1/2$.[11e,14,26,29] Although several Co(II)-containing radical complexes have been reported, only DC magnetic susceptibility measurements have been conducted, with no detailed studies on magnetization relaxation dynamics.[15b,30] In this context, a significant report by Boskovic, Soncini, and co-workers.[31] demonstrated that a high-spin octahedral Co(II) complex containing a semiquinone radical ligand, coupled antiferromagnetically, results in an integer spin state ($S = 1$). Similar to complex **1**, the reported system exhibits a field-induced slow relaxation phenomenon, with its relaxation process primarily governed by the Raman and Direct processes. In particular, to the best of our knowledge, there is only one square planar Co(II) low-spin complex that is reported to show slow relaxation of magnetisation. This must be associated with the synthetic challenge involved in the isolation of square planar geometry around cobalt system.[14b] In this respect, the reported complex **1** is a unique system that is stabilised by redox-active ligands that show slow relaxation of magnetisation.

Conclusions

The reaction of $[Co(PMe_3)_4]$ with the neutral ligand L1 in THF resulted in the isolation of a rare and unique square planar cobalt complex, $[Co^{II}(L1^{\bullet -})_2]$ (**1**), which was structurally characterized. Single-crystal X-ray diffraction analysis, combined with detailed CW-EPR and magnetic data modeling, confirmed that the cobalt ion in **1** adopts a divalent low-spin oxidation state. The square planar coordination environment is completed by two singly reduced radical anions of L1. The anisotropic g-tensors extracted from EPR and magnetic data revealed two key findings: (i) the spin density in **1** is localized predominantly on the Co^{II} ion, and (ii) the two radical anion ligands are coupled antiferromagnetically. The presence of ligand-based radicals was further corroborated by the observation of an intervalence charge transfer (IVCT) band in the UV-Vis spectrum. These experimental observations were strongly supported by theoretical calculations. Notably, complex **1** exhibits slow relaxation of magnetization, an exceedingly rare phenomenon for square planar Co^{II} complexes. The magnetization relaxation is dominated by Raman and direct processes. The combination of a doublet ground state and highly anisotropic g-tensor positions complex **1** as a promising candidate for molecular qubit applications. Further studies in this direction are currently underway.

Experimental Section

Materials and Methods

Unless otherwise mentioned, all the reactions were carried out under anaerobic conditions either using a glove box (Argon atmosphere) or Schlenk line techniques. Ligand L1 was synthesised following the literature procedure (see ESI for details).[15d] Single-crystal data were collected using a graphite monochromator on a Rigaku Saturn CCD diffractometer (MoK_α, $\lambda = 0.71073$ Å). The selected crystals were mounted on the tip of a glass pin using mineral oil and placed in the cold flow produced with an Oxford Cryo-cooling device. Structure solution and refinement were performed with the SHELX-package.[32] Structures were solved by direct methods and completed by iterative cycles of ΔF syntheses and full-matrix least-squares refinement against F^2 (CCDC: 2173864). The thermogravimetric analysis was performed on Hitachi NEXTA STA300 under N_2/Ar atmosphere. The dc susceptibility and magnetisation measurements were performed using a magnetic property measurement system (MPMS-XL SQUID Magnetometer) provided by Quantum Design, which is equipped with a 50 kOe superconducting magnet. Electron paramagnetic resonance (EPR) measurements were carried out using a Bruker EMX plus X-band EPR spectrometer operating in the continuous wave (CW) mode, equipped with an Oxford variable-temperature unit and an ESR900 cryostat with a Super High-Q resonator. Simulation of the CW-EPR spectra was performed using an Easy Spin toolbox (5.2.18).[16]

Computational Details

DFT calculation has been performed with B3LYP functional using the Gaussian09 suite.[33] The TZVP basis set was employed for the Co/Ni, and for all other elements 6–31G* basis set has been utilized.[34] A quadratic convergence method was employed to obtain the most stable wave function. TD-DFT calculations have been performed in acetonitrile employing the conductor-like polarisable continuum model (CPCM).[35] State-average CASSCF calculations have been performed along with a second-order N-electron perturbation theory method, as implemented in the ORCA 4.0.1 program package.[36] Scalar relativistic effects were included by the second-order Douglas—Kroll–Hess procedure.[37] Here, we have employed DKH-def2-TZVP basis set for Co, DKH-def2-TZVP(-f) basis set O and N, DKH-def2-SVP basis set for C and H. Initially, state average complete active space self-consistent field (CASSCF) calculations have been carried out with CAS(7,5) active space, i.e., seven electrons in five 3d orbitals. Thereafter, to include the dynamic correlation, N-electron valence perturbation theory (NEVPT2) calculations were performed on top of the SA-CASSCF wave functions.[38] Chemissian software has been used to make the frontier MO diagrams and to calculate the % contribution of metal and ligands.[39]

Synthesis of 1

In a 25 mL of Schlenk tube, 200 mg (0.544 mmol) of L1 was dissolved in 10 ml THF. Into this 98.85 mg (0.272 mmol) of [Co-(PMe_3)$_4$] was added. The colour of the solution changed immediately from light green to violet upon the addition of the Co(0) precursor. The resultant reaction mixture was stirred for about 16 h at room temperature. After completion of the reaction, the solution was filtered, and the filtrate was kept for crystallisation at room temperature in an Argon atmosphere. Upon slow evaporation, violet colour crystals were grown from filtrate after 48 hours which are ideal for single-crystal X-ray diffraction studies. The yield of **1** (based on [Co(PMe_3)$_4$]) = 26 mg (20%). Elemental analysis calculated (%): C, 78.67; H, 6.35; N, 3.53; found (%): C, 78.31; H, 5.94; N, 3.20.

Synthesis of 2

A similar synthetic procedure was employed to isolate **2**, but Ni(COD)$_2$ (74.85 mg; 0.272 mmol) was used instead of [Co(PMe_3)$_4$]. After completion of the reaction, green colour precipitate formation occurs. This was washed several times with THF and dried before being powder X-ray diffraction was performed. Yield (based on Ni(COD)$_2$): 150 mg (60%) Elemental analysis calculated (%): C, 78.69; H, 6.35; N, 3.53; found (%): C, 79.24; H, 5.85; N, 2.95.

Supporting Information

X-ray crystallographic parameters, polycrystalline EPR, XPS and DC data of 2, AILFT orbital splitting, and high-spin, spin density plots are provided in the electronic supplementary information. CCDC number: 2173864 The authors have cited additional references within the Supporting Information.[40]

Acknowledgements

MS thanks the funding agencies SERB (CRG/2023/002178), BRNS (58/14/07/2023-BRNS/37029), CSIR (01/3092/23/EMR-II) and IIT Bombay for the financial support. GR would like to thank SERB (CRG/2022/001697, SB/SJF/2019-20/12) for funding. Muralidharan Shanmugam (MS) thanks National EPSRC EPR service and facility (Grant REF: NS/A000055/1) and the University of Manchester for financial support. DB tanks to CSIR (09/087(1060)/2020-EMR–I) and IIT Bombay. AR thanks IITB for the financial assistance.

Conflict of Interests

The authors declare no conflict of interest.

Data Availability Statement

The data that support the findings of this study are available from the corresponding author upon reasonable request.

Keywords: cobalt · EPR · slow relaxation of magnetization · ab initio calculations · coordination complex

[1] a) J. L. Dempsey, B. S. Brunschwig, J. R. Winkler, H. B. Gray, *Acc. Chem. Res.* **2009**, *42*, 1995–2004; b) V. Fourmond, P.-A. Jacques, M. Fontecave, V. Artero, *Inorg. Chem.* **2010**, *49*, 10338–10347; c) A. Mahammed, B. Mondal, A. Rana, A. Dey, Z. Gross, *Chem. Commun.* **2014**, *50*, 2725–2727; d) H. Lei, A. Han, F. Li, M. Zhang, Y. Han, P. Du, W. Lai, R. Cao, *Phys. Chem. Chem. Phys* **2014**, *16*, 1883–1893; e) C. H. Lee, D. K. Dogutan, D. G. Nocera, *J. Am. Chem. Soc.* **2011**, *133*, 8775–8777; f) P.-A. Jacques, V. Artero, J. Pécaut, M. Fontecave, *Proc. Natl. Acad. Sci. U. S. A.*. **2009**, *106*, 20627–20632; g) X. Hu, B. S. Brunschwig, J. C. Peters, *J. Am. Chem. Soc.* **2007**, *129*, 8988–8998; h) P. Du, J. Schneider, G. Luo, W. W. Brennessel, R. Eisenberg, *Inorg. Chem.* **2009**, *48*, 4952–4962; i) J. L. Dempsey, J. R. Winkler, H. B. Gray, *J. Am. Chem. Soc.* **2010**, *132*, 16774–16776; j) A. Fihri, V. Artero, M. Razavet, C. Baffert, W. Leibl, M. Fontecave, *Angew. Chem.* **2008**, *120*, 574–577; k) V. Artero, M. Chavarot-Kerlidou, M. Fontecave, *Angew. Chem. Int. Ed.* **2011**, *50*, 7238–7266; l) V. Artero, M. Fontecave, *Chem. Soc. Rev.* **2013**, *42*, 2338–2356; m) T. S. Teets, D. G. Nocera, *Chem. Commun.* **2011**, *47*, 9268–9274.

[2] a) J. Devonport, L. Sully, A. K. Boudalis, S. Hassell-Hart, M. C. Leech, K. Lam, A. Abdul-Sada, G. J. Tizzard, S. J. Coles, J. Spencer, A. Vargas, G. E. Kostakis, *JACS Au* **2021**, *1*, 1937–1948; b) S. Chattopadhyay, A. Ghatak, Y. Ro, R. Guillot, Z. Halime, A. Aukauloo, A. Dey, *Inorg. Chem.* **2021**, *60*, 9442–9455; c) L.-L. Li, S.-S. Feng, T. Zhang, L. Wang, W.-K. Dong, *Inorg. Chim. Acta* **2022**, *534*, 120815; d) H. Oshita, Y. Shimazaki, *Molecules* **2022**, *27*; e) T. M. Rodriguez, M. Deegbey, E. Jakubikova, J. L. Dempsey, *Photosynth. Res.* **2022**, *151*, 155–161; f) T. Takeyama, T. Suzuki, M. Kikuchi, M. Kobayashi, H. Oshita, K. Kawashima, S. Mori, H. Abe, N. Hoshino, S. Iwatsuki, Y. Shimazaki, *Eur. J. Inorg. Chem.* **2021**, *2021*, 4133–4145; g) L.-L. Li, P. Li, T. Zhang, W.-K. Dong, *Polyhedron* **2021**, *205*, 115301; h) B. Speiser, G. Zitzer, *ChemElectroChem* **2021**, *8*, 2888–2902; i) P. Li, S.-Z. Li, Y.-X. Wei, W. K. Dong, *Polyhedron* **2021**, *204*, 115267; j) L.-L. Li, M. Li, P. Li, W.-K. Dong, *Inorg. Chim. Acta* **2021**, *520*, 120309; k) N. Leconte, F. Berthiol, C. Philouze, F. Thomas, *Eur. J. Inorg. Chem.* **2021**, *2021*, 1481–1489.

[3] a) G. J. P. Britovsek, V. C. Gibson, D. F. Wass, *Angew. Chem. Int. Ed.* **1999**, *38*, 428–447; b) G. J. P. Britovsek, V. C. Gibson, B. S. Kimberley, S. Mastroianni, C. Redshaw, G. A. Solan, A. J. P. White, D. J. Williams, *J. Chem. Soc., Dalton Trans.* **2001**, 1639–1644; c) J. V. Obligacion, P. J. Chirik, *J. Am. Chem. Soc.* **2013**, *135*, 19107–19110; d) A. M. Tondreau, S. C. E. Stieber, C. Milsmann, E. Lobkovsky, T. Weyhermüller, S. P. Semproni, P. J. Chirik, *Inorg. Chem.* **2013**, *52*, 635–646; e) G. Zhang, S. K. Hanson, *Org. Lett.* **2013**, *15*, 650–653; f) G. Zhang, S. K. Hanson, *Chem. Commun.* **2013**, *49*, 10151–10153; g) G. Zhang, K. V. Vasudevan, B. L. Scott, S. K. Hanson, *J. Am. Chem. Soc.* **2013**, *135*, 8668–8681; h) J. V. Obligacion, S. P. Semproni, P. J. Chirik, *J. Am. Chem. Soc.* **2014**, *136*, 4133–4136; i) S. K. Russell, J. M. Hoyt, S. C. Bart, C. Milsmann, S. C. E.

Stieber, S. P. Semproni, S. DeBeer, P. J. Chirik, *Chem. Sci.* **2014**, *5*, 1168–1174; j) S. P. Semproni, C. Milsmann, P. J. Chirik, *J. Am. Chem. Soc.* **2014**, *136*, 9211–9224.
[4] a) L. Huang, M. Arndt, K. Gooßen, H. Heydt, L. J. Gooßen, *Chem. Rev.* **2015**, *115*, 2596–2697; b) N. A. Ketterer, H. Fan, K. J. Blackmore, X. Yang, J. W. Ziller, M.-H. Baik, A. F. Heyduk, *J. Am. Chem. Soc.* **2008**, *130*, 4364–4374.
[5] V. Lyaskovskyy, B. de Bruin, *ACS Catal.* **2012**, *2*, 270–279.
[6] a) J. Scott, S. Gambarotta, I. Korobkov, Q. Knijnenburg, B. de Bruin, P. H. M. Budzelaar, *J. Am. Chem. Soc.* **2005**, *127*, 17204–17206; b) D. Enright, S. Gambarotta, G. P. A. Yap, P. H. M. Budzelaar, *Angew. Chem. Int. Ed.* **2002**, *41*, 3873–3876; c) N. H. Anderson, S. O. Odoh, Y. Yao, U. J. Williams, B. A. Schaefer, J. J. Kiernicki, A. J. Lewis, M. D. Goshert, P. E. Fanwick, E. J. Schelter, J. R. Walensky, L. Gagliardi, S. C. Bart, *Nat. Chem.* **2014**, *6*, 919–926; d) J. Scott, I. Vidyaratne, I. Korobkov, S. Gambarotta, P. H. M. Budzelaar, *Inorg. Chem.* **2008**, *47*, 896–911; e) J. Rajpurohit, M. Shanmugam, *Dalton Trans.* **2019**, *48*, 7378–7387.
[7] a) A. C. Bowman, C. Milsmann, E. Bill, E. Lobkovsky, T. Weyhermüller, K. Wieghardt, P. J. Chirik, *Inorg. Chem.* **2010**, *49*, 6110–6123; b) B. M. Wile, R. J. Trovitch, S. C. Bart, A. M. Tondreau, E. Lobkovsky, C. Milsmann, E. Bill, K. Wieghardt, P. J. Chirik, *Inorg. Chem.* **2009**, *48*, 4190–4200.
[8] Q. Knijnenburg, D. Hetterscheid, T. M. Kooistra, H. M. Budzelaar, *Eur. J. Inorg. Chem.* **2004**, *2004*, 1204–1211.
[9] a) C. Bunting Philip, M. Atanasov, E. Damgaard-Møller, M. Perfetti, I. Crassee, M. Orlita, J. Overgaard, J. van Slageren, F. Neese, R. Long Jeffrey, *Science* **2018**, *362*, eaat7319; b) X.-N. Yao, J.-Z. Du, Y.-Q. Zhang, X.-B. Leng, M.-W. Yang, S.-D. Jiang, Z.-X. Wang, Z.-W. Ouyang, L. Deng, B.-W. Wang, S. Gao, *J. Am. Chem. Soc.* **2017**, *139*, 373–380; c) S. Vaidya, S. Tewary, S. K. Singh, S. K. Langley, K. S. Murray, Y. Lan, W. Wernsdorfer, G. Rajaraman, M. Shanmugam, *Inorg. Chem.* **2016**, *55*, 9564–9578; d) M. Murrie, *Chem. Soc. Rev.* **2010**, *39*, 1986–1995.
[10] a) J. Ferrando-Soria, E. Moreno Pineda, A. Chiesa, A. Fernandez, S. A. Magee, S. Carretta, P. Santini, I. J. Vitorica-Yrezabal, F. Tuna, G. A. Timco, E. J. L. McInnes, R. E. P. Winpenny, *Nat. Commun.* **2016**, *7*, 11377; b) A. Ardavan, O. Rival, J. J. L. Morton, S. J. Blundell, A. M. Tyryshkin, G. A. Timco, R. E. P. Winpenny, *Phys. Rev. Lett.* **2007**, *98*, 057201; c) R. E. P. Winpenny, *Angew. Chem. Int. Ed.* **2008**, *47*, 7992–7994.
[11] a) J. M. Zadrozny, J. Niklas, O. G. Poluektov, D. E. Freedman, *ACS Cent. Sci.* **2015**, *1*, 488–492; b) C.-J. Yu, M. J. Graham, J. M. Zadrozny, J. Niklas, M. D. Krzyaniak, M. R. Wasielewski, O. G. Poluektov, D. E. Freedman, *J. Am. Chem. Soc.* **2016**, *138*, 14678–14685; c) J. M. Zadrozny, M. J. Graham, M. D. Krzyaniak, M. R. Wasielewski, D. E. Freedman, *Chem. Commun.* **2016**, *52*, 10175–10178; d) M. J. Graham, C.-J. Yu, M. D. Krzyaniak, M. R. Wasielewski, D. E. Freedman, *J. Am. Chem. Soc.* **2017**, *139*, 3196–3201; e) M. Atzori, L. Tesi, E. Morra, M. Chiesa, L. Sorace, R. Sessoli, *J. Am. Chem. Soc.* **2016**, *138*, 2154–2157; f) M. Atzori, E. Morra, L. Tesi, A. Albino, M. Chiesa, L. Sorace, R. Sessoli, *J. Am. Chem. Soc.* **2016**, *138*, 11234–11244.
[12] a) M. J. Amdur, K. Mullin, M. Waters, D. Puggioni, M. Wojnar, M. Gu, L. Sun, P. Oyala, J. Rondinelli, D. Freedman, *Chem. Sci.* **2022**; b) L. C. de Camargo, M. Briganti, F. S. Santana, D. Stinghen, R. R. Ribeiro, G. G. Nunes, J. F. Soares, E. Salvadori, M. Chiesa, S. Benci, *Angew. Chem.* **2021**, *133*, 2620–2625.
[13] a) C.-J. Yu, M. D. Krzyaniak, M. S. Fataftah, M. R. Wasielewski, D. E. Freedman, *Chem. Sci.* **2019**, *10*, 1702–1708; b) M.-X. Xu, Z. Liu, B.-W. Dong, H.-H. Cui, Y.-X. Wang, J. Su, Z. Wang, Y. Song, X.-T. Chen, S.-D. Jiang, S. Gao, *Inorg. Chem.* **2019**, *58*, 2330–2335.
[14] a) L. Spillecke, S. Tripathi, C. Koo, A. Bahr, A. Swain, R. Haldar, M. Ansari, J. Jasinski, G. Rajaraman, M. Shanmugam, R. Klingeler, *Inorg. Chem.* **2022**, *61*, 317–327; b) I. Bhowmick, D. W. Shaffer, J. Y. Yang, M. P. Shores, *Chem. Commun.* **2020**, *56*, 6711–6714; c) H.-H. Cui, J. Wang, X.-T. Chen, Z.-L. Xue, *Chem. Commun.* **2017**, *53*, 9304–9307.
[15] a) E. Bill, E. Bothe, P. Chaudhuri, K. Chlopek, D. Herebian, S. Kokatam, K. Ray, T. Weyhermüller, F. Neese, K. Wieghardt, *Chem. Eur. J.* **2005**, *11*, 204–224; b) A. I. Poddel'sky, V. K. Cherkasov, G. K. Fukin, M. P. Bubnov, L. G. Abakumova, G. A. Abakumov, *Inorg. Chim. Acta* **2004**, *357*, 3632–3640; c) L. A. Cameron, J. W. Ziller, A. F. Heyduk, *Chem. Sci.* **2016**, *7*, 1807–1814; d) B. Xu, A. Ma, T. Jia, Z. Hao, W. Gao, Y. Mu, *Dalton Trans.* **2016**, *45*, 17966–17973; e) B. Gao, X. Luo, W. Gao, L. Huang, S.-m. Gao, X. Liu, Q. Wu, Y. Mu, *Dalton Trans.* **2012**, *41*, 2755–2763.
[16] a) M. A. Hemminga, L. J. Berliner, Editors, *ESR Spectroscopy in Membrane Biophysics. (Biological Magnetic Resonance, Vol. 27)*, Kluwer, **2007**; b) S. Stoll, A. Schweiger, *J. Magn. Reson.* **2006**, *178*, 42–55.
[17] a) H. Kanso, R. M. Clarke, A. Kochem, H. Arora, C. Philouze, O. Jarjayes, T. Storr, F. Thomas, *Inorg. Chem.* **2020**, *59*, 5133–5148; b) V. M. Krishnan, I. Davis, T. M. Baker, D. J. Curran, H. D. Arman, M. L. Neidig, A. Liu, Z. J. Tonzetich, *Inorg. Chem.* **2018**, *57*, 9544–9553; c) Z. Mo, Y. Li, H. K. Lee, L. Deng, *Organometallics* **2011**, *30*, 4687–4694; d) S. Dey, B. B. Wayland, M. J. Zdilla, *Inorg. Chem.* **2019**, *58*, 1224–1233.
[18] a) Y. S. Chen, J. F. Kang, B. Chen, B. Gao, L. F. Liu, X. Y. Liu, Y. Y. Wang, L. Wu, H. Y. Yu, J. Y. Wang, Q. Chen, E. G. Wang, *J. Phys. D: Appl. Phys.* **2012**, *45*, 065303; b) L. Mi, W. Wei, S. Huang, S. Cui, W. Zhang, H. Hou, W. Chen, *J. Mater. Chem. A* **2015**, *3*, 20973–20982.
[19] R. P. Yu, J. M. Darmon, C. Milsmann, G. W. Margulieux, S. C. E. Stieber, S. DeBeer, P. J. Chirik, *J. Am. Chem. Soc.* **2013**, *135*, 13168–13184.
[20] a) S. A. Carabineiro, L. C. Silva, P. T. Gomes, L. C. J. Pereira, L. F. Veiros, S. I. Pascu, M. T. Duarte, S. Namorado, R. T. Henriques, *Inorg. Chem.* **2007**, *46*, 6880–6890; b) S. Murugesan, B. Stöger, M. D. Carvalho, L. P. Ferreira, E. Pittenauer, G. Allmaier, L. F. Veiros, K. Kirchner, *Organometallics* **2014**, *33*, 6132–6140.
[21] a) Y. F. Song, G. A. van Albada, M. Quesada, I. Mutikainen, U. Turpeinen, J. Reedijk, *Inorg. Chem. Commun.* **2005**, *8*, 975–978; b) O. Kahn, *Molecular magnetism*, Courier Dover Publications, **2021**.
[22] a) D. Herebian, E. Bothe, F. Neese, T. Weyhermüller, K. Wieghardt, *J. Am. Chem. Soc.* **2003**, *125*, 9116–9128; b) D. Herebian, K. E. Wieghardt, F. Neese, *J. Am. Chem. Soc.* **2003**, *125*, 10997–11005.
[23] S. Ye, F. Neese, *Inorg. Chem.* **2010**, *49*, 772–774.
[24] K. Ray, A. Begum, T. Weyhermüller, S. Piligkos, J. van Slageren, F. Neese, K. Wieghardt, *J. Am. Chem. Soc.* **2005**, *127*, 4403–4415.
[25] A. J. McNeece, K. A. Jesse, J. Xie, A. S. Filatov, J. S. Anderson, *J. Am. Chem. Soc.* **2020**, *142*, 10824–10832.
[26] a) A. B. Buades, V. S. Arderiu, L. Maxwell, M. Amoza, D. Choquesillo-Lazarte, N. Aliaga-Alcalde, C. Viñas, F. Teixidor, E. Ruiz, *Chem. Commun.* **2019**, *55*, 3825–3828; b) R. C. Poulten, M. J. Page, A. G. Algarra, J. J. Le Roy, I. López, E. Carter, A. Llobet, S. A. Macgregor, M. F. Mahon, D. M. Murphy, M. Murugesu, M. K. Whittlesey, *J. Am. Chem. Soc.* **2013**, *135*, 13640–13643.
[27] a) K. S. Cole, R. H. Cole, *J. Chem. Phys.* **1941**, *9*, 341–351; b) K. S. Cole, R. H. Cole, *J. Chem. Phys.* **1942**, *10*, 98–105; c) Y.-N. Guo, G.-F. Xu, Y. Guo, J. Tang, *Dalton Trans.* **2011**, *40*, 9953–9963.
[28] a) S. Vaidya, P. Shukla, S. Tripathi, E. Rivière, T. Mallah, G. Rajaraman, M. Shanmugam, *Inorg. Chem.* **2018**, *57*, 3371–3386; b) C. Das, A. Rasamsetty, S. Tripathi, M. Shanmugam, *Chem. Commun.* **2020**, *56*, 13397–13400.
[29] a) Q.-Q. Su, K. Fan, X.-D. Huang, J. Xiang, S.-C. Cheng, C.-C. Ko, L.-M. Zheng, M. Kurmoo, T.-C. Lau, *Dalton Trans.* **2020**, *49*, 4084–4092; b) R. Boča, C. Rajnák, J. Titiš, D. Valigura, *Inorg. Chem.* **2017**, *56*, 1478–1482.
[30] a) S. J. Bonyhady, J. M. Goldberg, N. Wedgwood, T. R. Dugan, A. G. Eklund, W. W. Brennessel, P. L. Holland, *Inorg. Chem.* **2015**, *54*, 5148–5150; b) D. G. Brown, T. Maier, R. S. Drago, *Inorg. Chem.* **1971**, *10*, 2804–2806; c) K. E. Preuss, *Coord. Chem. Rev.* **2015**, *289–290*, 49–61; d) Q. H. Zhao, D. Y. Tang, Y. H. Zhang, R. B. Fang, *Russ. J. Coord. Chem.* **2006**, *32*, 261–265.
[31] G. K. Gransbury, M.-E. Boulon, R. A. Mole, R. W. Gable, B. Moubaraki, K. S. Murray, L. Sorace, A. Soncini, C. Boskovic, *Chem. Sci.* **2019**, *10*, 8855–8871.
[32] G. M. Sheldrick, C. J. Gilmore, H. A. Hauptman, C. M. Weeks, R. Miller, I. Usón, *ShelX*, Wiley Online Library, **2012**.
[33] M. J. Frisch, http://www. gaussian. com/ **2009**.
[34] a) A. Schäfer, C. Huber, R. Ahlrichs, *J. Chem. Phys.* **1994**, *100*, 5829–5835; b) F. Weigend, R. Ahlrichs, *Phys. Chem. Chem. Phys* **2005**, *7*, 3297–3305.
[35] a) V. Barone, M. Cossi, *J. Phys. Chem. A* **1998**, *102*, 1995–2001; b) M. Cossi, V. Barone, *J. Chem. Phys.* **2001**, *115*, 4708–4717; c) M. Cossi, N. Rega, G. Scalmani, V. Barone, *J. Comput. Chem.* **2003**, *24*, 669–681.
[36] a) F. Neese, *Wiley Interdiscip. Rev. Comput. Mol. Sci.* **2012**, *2*, 73–78; b) C. Angeli, R. Cimiraglia, J.-P. Malrieu, *Chem. Phys. Lett.* **2001**, *350*, 297–305.
[37] B. A. Hess, *Phys. Rev. A* **1986**, *33*, 3742–3748.
[38] C. Angeli, R. Cimiraglia, S. Evangelisti, T. Leininger, J. P. Malrieu, *J. Chem. Phys.* **2001**, *114*, 10252–10264.
[39] L. Skripnikov, *For the current version, see www. chemissian. com* **2012**.
[40] X-ray crystallographic parameters, polycrystalline EPR, XPS and DC data of 2, AILFT orbital splitting and high-spin, spin density plots are provided in the electronic supplementary information.

Manuscript received: December 6, 2024
Revised manuscript received: February 20, 2025
Accepted manuscript online: March 6, 2025
Version of record online: March 24, 2025